J. metamorphic Geol., 1996, **14,** 427–440

Temperature–time path for the low-pressure Ryoke metamorphism, Japan, based on chemical zoning in garnet

T. OKUDAIRA*
Department of Earth and Planetary Systems Science, Faculty of Science, Hiroshima University, 1–3–1 Kagamiyama, Higashi-Hiroshima 739, Japan (email: oku@geol.sci.hiroshima-u.ac.jp)

ABSTRACT Garnet crystals from low-pressure/high-temperature (LPHT) Ryoke metamorphic rocks in the Yanai district, south-western Japan, show several kinds of chemical zoning patterns that systematically vary with grain radius between *c.* 0.1 and 0.5 mm. Large grains ($>c.$ 0.4 mm) show normal zoning and small grains ($<c.$ 0.4 mm) show unzoned or reversely zoned cores. Observations of the chemical zoning and of the spatial and size distributions of the garnet grains between *c.* 0.1 and 0.5 mm in radius suggest that they were formed by continuous nucleation and diffusion-controlled growth.

A previously estimated temperature–time path (T–t path) for the Ryoke metamorphism, using 1-D numerical simulation, is characterized by a rapid increase in temperature, 0.0017 °C yr^{-1} on average, and a period of high temperature (>600 °C) shorter than 0.5 Myr, which was presumably caused by the intrusion of a granodiorite sheet. Chemical zoning of garnet grains with different radii simulated for the T–t path using a numerical model of continuous nucleation and diffusion-controlled growth, in combination with intracrystalline diffusion, compares well with the observed zoning patterns in garnet grains with different radii. This is in spite of the fact that the simulated zoning patterns vary greatly, depending on subtle differences in the T–t history. Therefore, they suggest that the T–t path gives a good explanation for the LPHT Ryoke metamorphism. Although this study only refers to the Ryoke metamorphism, the technique may be applicable to thermal modelling of other metamorphic terranes.

Key words: chemical zoning; diffusion-controlled growth; garnet; intracrystalline diffusion; Ryoke metamorphic belt; temperature–time path.

INTRODUCTION

Thermal evolution during metamorphism and associated tectonism has been interpreted in a number of metamorphic terranes on the basis of numerical thermal modelling (e.g. Oxburgh & Turcotte, 1971; Wells, 1980; England & Thompson, 1984; Lux *et al.*, 1986; Wickham & Oxburgh, 1987; De Yoreo *et al.*, 1989; Loosveld, 1989; Rothstein & Hoisch, 1994). However, petrological evaluation of the modelling has not been well documented.

Growth zoning occurs as new shells of different composition are added onto a growing crystal. The compositional differences in the shells arise because of changing external conditions, such as pressure and temperature. Therefore, it has been considered that chemical zoning in a metamorphic garnet records the P–T history of metamorphism (e.g. Loomis & Nimick, 1982; Spear, 1989a,b; Florence & Spear, 1991, 1993). 'Normal' zoning in garnet, involving decrease of Mn content from centre to margin, has been interpreted as a result of continuous growth with increasing temperature (e.g. Loomis & Nimick, 1982; Spear, 1988). In contrast, garnet crystals with unzoned cores have been reported from many high-T metamorphic terranes (e.g. Yardley, 1977; Tracy, 1982; Dempster, 1985; Ikeda, 1993a,b). They have been interpreted to have formed by intracrystalline diffusion (volume diffusion) obliterating the pre-existing chemical zoning during metamorphism (e.g. Tracy, 1982; Loomis, 1983; Dempster, 1985; Chakraborty & Ganguly, 1990; Spear, 1991) or by rapid growth of the garnet (Hodges & Silverberg, 1988). Intracrystalline diffusion more effectively relaxes the zoning pattern when a crystal is smaller, metamorphic temperature is higher and duration of the metamorphism is longer (e.g. Loomis, 1983; Chakraborty & Ganguly, 1990; Florence & Spear, 1991). Preservation of normal zoning in garnet may therefore mean that the growth was slow enough for the zoning to appear, and that the temperature and/or the duration of the metamorphism were not high and/or long enough to obliterate the pre-existing zoning by intracrystalline diffusion. Thus, when nucleation and growth mechanisms of garnet crystals are identified, chemical zoning can be used to examine the pressure–temperature–time path (P–T–t path) of metamorphism (Spear, 1989a,b; Chakraborty & Ganguly, 1990; Florence & Spear, 1991, 1993).

In this paper, I present chemical zoning profiles in garnet from the Ryoke metamorphic rocks in the

*Present address: Geological Institute, School of Science, University of Tokyo, 7-3-1 Hongo, Tokyo 113, Japan.

Yanai district, south-western Japan, and compare them with numerically simulated zoning patterns. Then the temperature–time path (T–t path) of the low-P Ryoke metamorphism proposed by Okudaira *et al.* (1994) is examined.

BACKGROUND

Geological setting

The Ryoke metamorphic belt (Fig. 1a), which consists of abundant granitoids and an associated low-P/high-T (LPHT) type metamorphic complex, is a typical low-P metamorphic belt (e.g. Miyashiro, 1961). The E–W-trending Ryoke metamorphic belt is juxtaposed against the E–W-trending high-P Sambagawa metamorphic belt at the Median Tectonic Line (MTL) in south-western Japan. The age of metamorphism in both belts is Cretaceous (e.g. Banno & Nakajima, 1992; Nakajima, 1994).

The Yanai district (Fig. 1b) is mainly composed of granitoids (the Ryoke and Hiroshima granitoids) and associated metamorphic rocks (the Ryoke metamorphic rocks) of Middle Cretaceous age (e.g. Nureki, 1960; Okamura, 1960; Higashimoto *et al.*, 1983; Hara *et al.*, 1991; Ikeda, 1991, 1993a; Okudaira *et al.* 1993; Nakajima, 1994). The granitoids have been divided into two categories (Fig. 1b): sheet-like granitoids (the

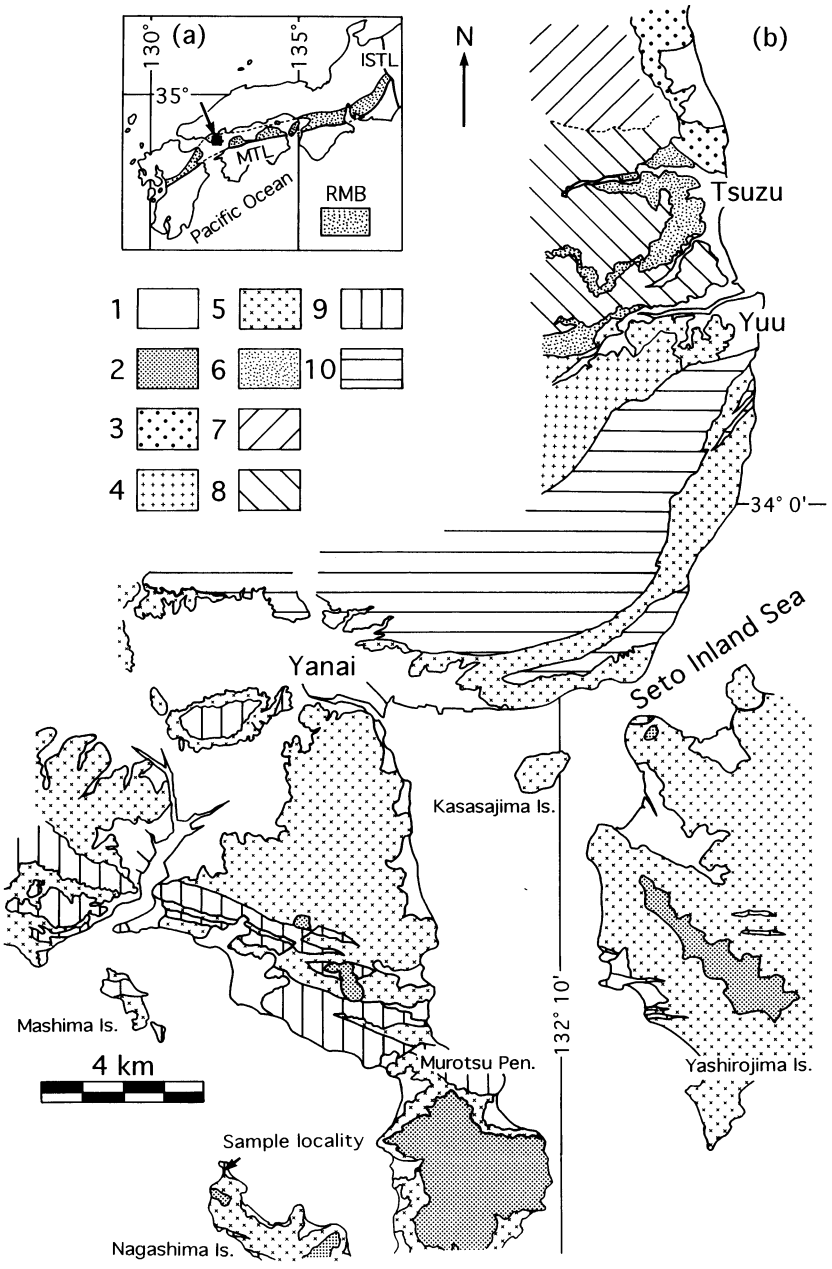

Fig. 1. (a) Outline map showing the location of the Ryoke metamorphic belt of south-western Japan. RMB, Ryoke metamorphic belt; MTL, Median Tectonic Line; ISTL, Itoigawa-Shizuoka Tectonic Line. (b) Geological and metamorphic zonation map of the Yanai district, south-western Japan. 1, alluvium; 2, Tertiary volcanics; 3, Hiroshima granitoid; 4, Younger Ryoke granitoid; 5, Older Ryoke granitoid; 6, agmatic migmatite zone; 7–10, Ryoke metamorphic rocks (7 biotite zone, 8 cordierite zone, 9 sillimanite zone, 10 garnet zone.)

Older Ryoke granitoids) and stock-like granitoids (the Younger Ryoke and Hiroshima granitoids) by Higashimoto *et al.* (1983), Hara *et al.* (1991) and Okudaira *et al.* (1993). Because their mineralogical and chemical features are those of metaluminous I-type granitoids, they are believed to be derived from the lower crust and upper mantle, rather than having been generated *in situ* in the middle crust (e.g. Honma, 1974; Kagami *et al.*, 1992).

Following Okudaira *et al.* (1993, 1995), the Ryoke metamorphic rocks are divided into four M1 metamorphic zones (Fig. 1b): biotite zone, cordierite zone (460–590 °C, 2.5–3.5 kbar), sillimanite zone (630–690 °C, 3.0–5.0 kbar) and garnet zone (730–770 °C, 5.5–6.5 kbar). Some residual minerals, such as corundum, sillimanite, garnet and Zn-rich hercynite, in a few xenoliths of the agmatic migmatite zone have been inferred to be evidence of pre-M1 metamorphism (M0) (Okudaira *et al.*, 1993). After M1, the stock-like granitoids intruded and locally metamorphosed the surrounding rocks (M2) in the north of the area (Fig. 1b). Because there is no evidence of M0 and M2 in the analysed sample from the sillimanite zone, M0 and M2 are not discussed in the following sections.

Estimated *T–t* path

M1 metamorphism has a strong temporal and spatial correlation with emplacement of the Older Ryoke granitoid, as indicated by the following evidence. (1) The distribution of the granitoid correlates with that of the sillimanite and garnet zones. (2) Throughout the high-grade metamorphic zones, distinct contact aureoles caused by the intrusion of the granitoid are lacking. (3) Structures of the high-grade metamorphic rocks are concordant with those of the granitoid. (4) Radiometric ages of the metamorphic rocks are compatible with those of the granitoid (Shigeno & Yamaguchi, 1976; Higashimoto *et al.*, 1983; Banno & Nakajima, 1992; Nakajima *et al.*, 1993; Nakajima, 1994; Suzuki *et al.*, 1994). These relationships suggest that M1 resulted from the intrusion of the Older Ryoke granitoid (Okudaira *et al.*, 1993, 1994), and a probable *T–t* path for M1 was proposed by Okudaira *et al.* (1994), based on a 1-D numerical simulation (Fig. 2; Appendix). The *T–t* paths of rocks that reached the sillimanite zone are characterized by a rapid increase in temperature, 0.0017 °C yr^{-1} on average, and a period of high temperature (>600 °C) shorter than 0.5 Myr. According to the model, the peak temperature (670 °C) was attained 0.1 Myr after the intrusion of the Older Ryoke granitoid. Since the thermal relaxation was fast, the geotherm recovered to a nearly steady state after *c.* 5 Myr.

EXPERIMENTAL PROCEDURE

Garnet crystals were separated following the methods of Kretz (1973) and Banno *et al.* (1986) from a small volume (about 4 cm^3) of metapelite from the sillimanite zone (Fig. 1b). The rock was heated in air to 700 °C for 60 min, quenched in water and pressed in a vice. Garnet crystals were separated from other minerals using tweezers. Approximately 80–90% of the garnet crystals could be extracted without breaking. Idioblastic crystals were mounted in resin. The mount was ground down and polished until the crystal diameter seen in the petrographic microscope was equal to that seen in the reflecting microscope. By this procedure, a good polished section of garnet through its centre was obtained.

Separated garnet crystals were analysed using an electron-probe microanalyser (JEOL, JCMA-733II) at Hiroshima University, operating at an accelerating voltage of 15 kV, a current of 19 nA and a beam width of 5 μm.

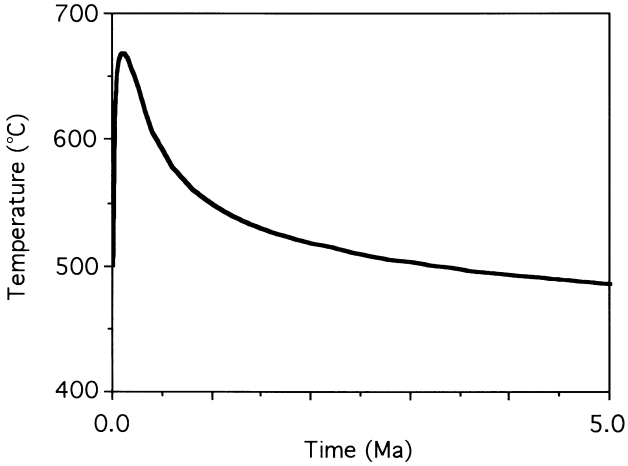

Fig. 2. *T–t* path for the sillimanite zone, calculated by 1-D numerical simulation (Okudaira *et al.*, 1994).

CHEMICAL ZONING IN GARNET

The studied metapelite of the sillimanite zone (Fig. 1b) is composed of alternating, mica-rich and mica-poor layers (a few millimetres thick). Quartz, plagioclase, K-feldspar, biotite, sillimanite, garnet and cordierite are present, though cordierite is rare and does not coexist with garnet. Graphite, ilmenite, apatite, zircon and tourmaline occur as minor minerals. A typical mineral assemblage in the zone is shown on Thompson's (1957) A′FM diagram in Fig. 3.

Garnet crystals in the metapelite are idioblastic or subidioblastic (Fig. 4a,d), although some large crystals are xenoblastic where they grew together (Fig. 4b,c). Garnet crystals smaller than *c.* 0.5 mm in radius are concentrated in mica-poor layers, whereas garnet crystals larger than *c.* 0.5 mm in radius are sparsely dispersed in mica-rich layers. Almost all the garnet crystals show textural zoning, which consists of inclusion-rich core and inclusion-poor rim (Fig. 4). The inclusions, which are mostly xenoblastic quartz and a very small amount of graphite, ilmenite and

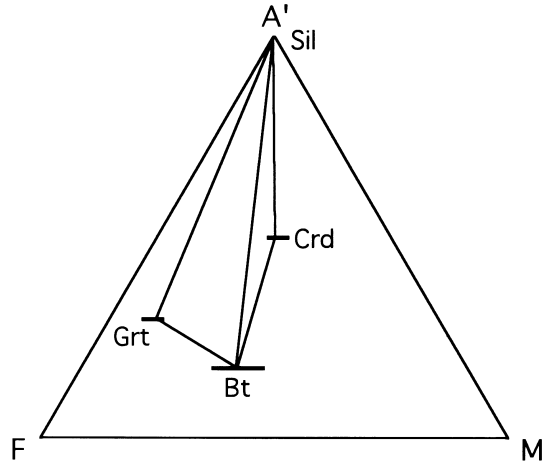

Fig. 3. A′FM diagram projected from K-feldspar in Thompson's AKFM system for the sillimanite zone.

biotite, show no distinct alignment and do not show evidence of rotation, which indicates static crystallization of the garnet (e.g. Spry, 1969; Barker, 1990). The boundary between the inclusion-rich core and inclusion-poor rim is commonly parallel to the faces of the garnet crystal (Fig. 4c). There is no relationship between the textural and chemical zonings.

Representative chemical compositions of the garnet are presented in Table 1. The chemical zoning profiles of molar fractions of almandine (X_{Fe}), spessartine (X_{Mn}), pyrope (X_{Mg}), and grossular (X_{Ca}) in metapelitic garnet grains with radii between 0.1 and 0.8 mm at *c.* 0.1-mm intervals are shown in Fig. 5. These profiles were measured from the geometrical centre to the outermost margin. The garnet was regarded as lacking chemical zoning where variation in spessartine content was <1 mol% within a single grain, except for the reversely zoned part.

With regard to the profiles of spessartine (X_{Mn}), important features in Fig. 5 are as follows.

1 Three kinds of garnet with normally zoned, unzoned and reversely zoned patterns in their cores occur together in the metapelitic unit.

2 Sample A (radius: $r=0.10$ mm) is reversely zoned from the centre to outermost margin (Fig. 5a).

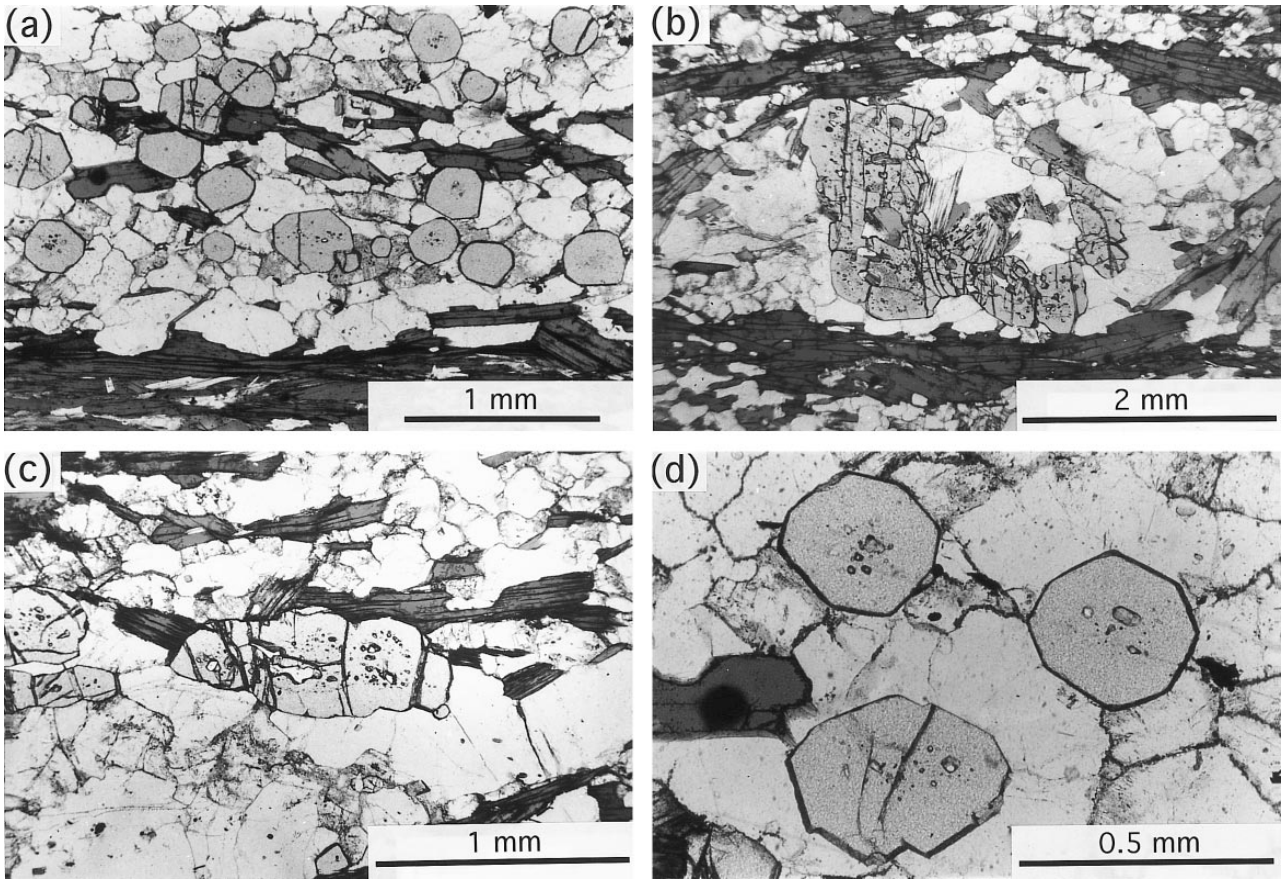

Fig. 4. Textures of garnet crystals in the studied metapelite. Grains with high refractive index are garnet. Dark-coloured and light-coloured minerals are biotite and felsic minerals (quartz, plagioclase and K-feldspar), respectively. Plane-polarized light. (a) Idioblastic to subidioblastic garnet crystals preferentially concentrated in mica-poor layer. (b) and (c) Xenoblastic garnet grains showing a texture suggesting impingement of more than two crystals. (d) Idioblastic garnet crystals with quartz inclusion in their cores.

Table 1. Chemical compositions at the geometrical centre (left column) and outermost margin (right column) of garnets in cations per mineral formula (O = 24). Radius (mm) of each sample is given in parentheses.

Sample no.	A (0.10 mm)		B (0.20 mm)		C (0.32 mm)		D (0.44 mm)		E (0.50 mm)		F (0.56 mm)		G (0.70 mm)		H (0.80 mm)	
Si	6.03	6.02	6.02	6.06	6.00	5.99	5.97	5.95	5.98	5.95	6.03	6.07	5.96	5.85	5.93	5.98
Al	4.04	4.04	4.05	4.13	4.04	4.07	4.05	4.05	4.03	4.09	4.01	4.07	4.07	4.06	4.07	4.16
Fe	4.18	4.19	4.20	3.93	4.17	4.07	4.17	4.20	3.95	4.12	3.91	3.96	3.83	4.20	4.21	3.95
Mn	0.84	1.11	0.88	1.11	0.95	1.21	1.03	1.15	1.25	1.16	1.25	1.20	1.35	1.25	1.03	1.24
Mg	0.59	0.46	0.57	0.46	0.56	0.42	0.54	0.47	0.47	0.47	0.45	0.41	0.42	0.43	0.52	0.40
Ca	0.25	0.22	0.24	0.19	0.26	0.19	0.24	0.21	0.32	0.21	0.31	0.19	0.38	0.24	0.29	0.22
Sum	15.93	16.04	15.96	15.88	15.98	15.95	16.00	16.03	16.00	16.00	15.96	15.90	16.01	16.03	16.05	15.95
$*X_{Fe+Mn}$	0.86	0.89	0.86	0.89	0.86	0.90	0.87	0.89	0.87	0.89	0.87	0.90	0.87	0.89	0.87	0.89

$* X_{Fe+Mn} = (Fe + Mn)/(Fe + Mn + Mg + Ca)$.

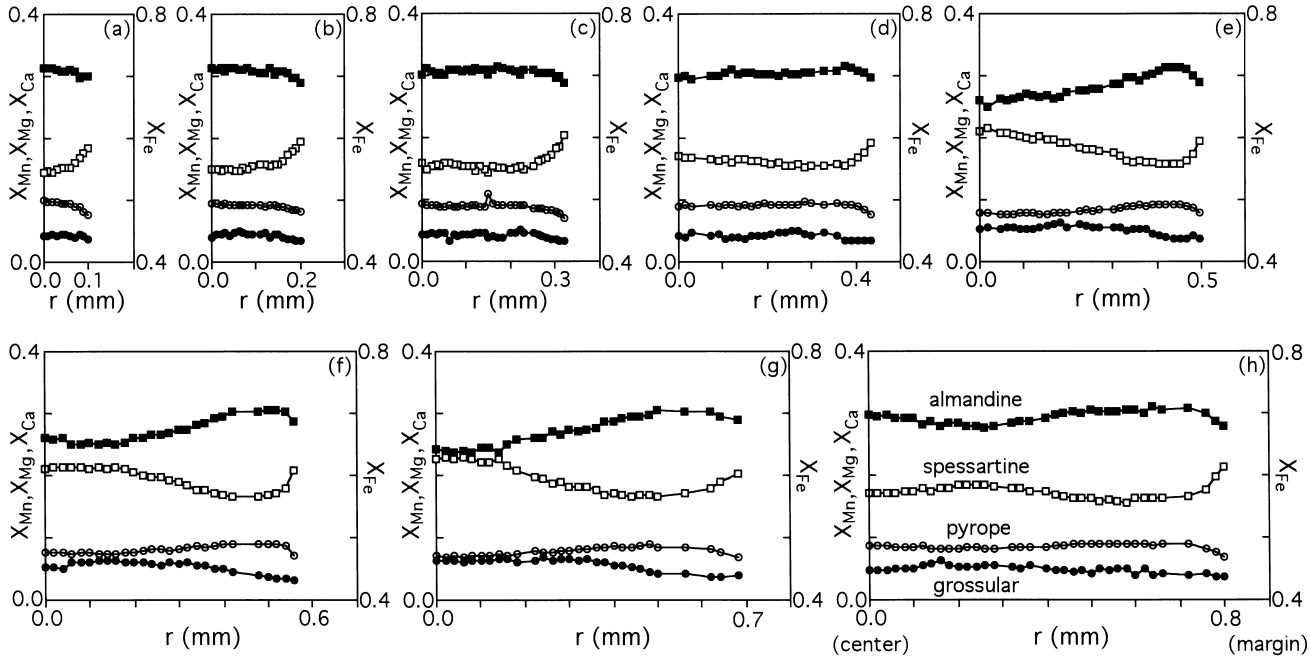

Fig. 5. Chemical zoning patterns for almandine (X_{Fe}), spessartine (X_{Mn}), pyrope (X_{Mg}) and grossular (X_{Ca}) of the separated garnet crystals with radii between 0.1 and 0.8 mm at *c.* 0.1-mm intervals. (a) Sample A ($r = 0.10$ mm); (b) sample B ($r = 0.20$ mm); (c) sample C ($r = 0.32$ mm); (d) sample D ($r = 0.44$ mm); (e) sample E ($r = 0.50$ mm); (f) sample F ($r = 0.56$ mm); (g) sample G ($r = 0.70$ mm); (h) sample H ($r = 0.80$ mm).

3 Samples B ($r = 0.20$ mm) and C ($r = 0.32$ mm) consist of unzoned cores and reversely zoned rims (Fig. 5b,c).
4 Samples D ($r = 0.44$ mm), E ($r = 0.50$ mm), F ($r = 0.56$ mm) and G ($r = 0.70$ mm) consist of normally zoned cores and reversely zoned rims (Fig. 5d–g).
5 Sample H ($r = 0.80$ mm) does not show an X_{Mn} maximum at its centre (Fig. 5h), but shows multiple peaks of X_{Mn}, as reported by Ikeda (1993a,b).
6 The width of the reversely zoned part in garnet grains with radii smaller than 0.70 mm is ≈ 0.1 mm, whereas that of reversely zoned parts in grains of 0.70 and 0.80 mm in radius is *c.* 0.2 mm.

The molar fraction of spessartine (X_{Mn}) at the centre of garnet grains (solid squares in Fig. 6) continuously increases with an increase in radius, except for the larger ($r > 0.5$ mm) grains, in which the X_{Mn} varies greatly. Since the X_{Mn} in the larger ($r > 0.5$ mm) grains is more variable, the zoning profiles for the larger grains shown in Fig. 5(f–h) are not representative of their grain sizes. In contrast, X_{Mn} at the outermost margins (open squares in Fig. 6) does not vary with grain size, ranging between *c.* 0.18 and 0.22 (mean value *c.* 0.2).

NUCLEATION AND GROWTH MECHANISMS OF GARNET

Nucleation and growth mechanisms of crystals are reflected in textural features, such as spatial and size distributions, which are recorded in the rock at the end of the crystallization episode (e.g. Kerrick *et al.*, 1991). The crystal size distribution (CSD) plot (Cashman & Ferry, 1988) for garnet in the metapelite is shown in Fig. 7. This plot was made by the following procedures. Using an optical microscope with a micrometer, I measured the size of all the garnet grains ($n = 504$) in two thin sections (total measured area 14 cm^2) from the same metapelite for which the chemical zoning in garnet was studied. Following

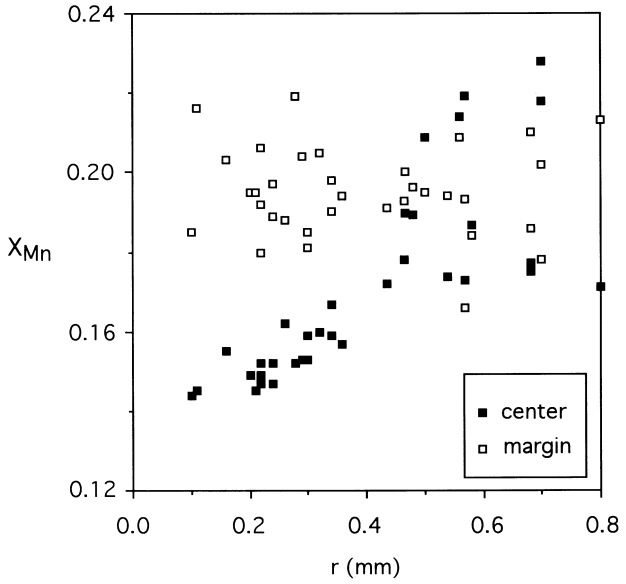

Fig. 6. X_{Mn} values at geometrical centres (solid squares) and outermost margins (open squares) of garnet grains from the metapelite.

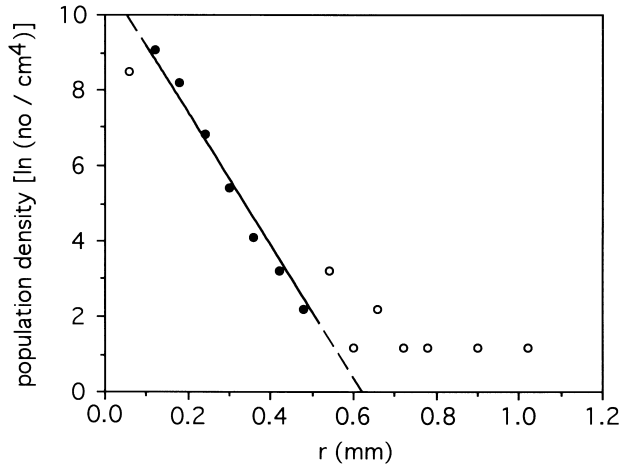

Fig. 7. CSD plot for garnet grains of metapelite.

Cashman & Ferry (1988) and Morishita (1992), the number of garnet grains per size class and unit area (N_a) is expressed by $N_a = c/(a\ \Delta L)$, where c, a and ΔL are the number of garnet crystals within the size class, measured area and size class (0.06 mm in this study), respectively. The number of crystals per size class and per unit volume (N_v) is represented by $N_v = (c/a)^{1.5}/\Delta L$ (Cashman & Ferry, 1988; Morishita, 1992). In Fig. 7, the CSD plot shows that crystals of the intermediate size classes, from 0.12 to 0.48 mm (solid circles), fit a line with a slope of 5.68×10^{-3} cm (solid line). The linear crystal size distribution suggests that the crystals continuously nucleated and grew (Cashman & Ferry, 1988; Carlson, 1989; Kerrick *et al.*, 1991). The continuous increase in X_{Mn} at the centre of garnet grains with radius between 0.1 and 0.5 mm (Fig. 6) also indicates that garnet continuously nucleated and grew during the prograde metamorphism, because X_{Mn} at the centre of garnet grains is inferred to reflect the P–T conditions at the time of nucleation (e.g. Loomis & Nimick, 1982; Spear, 1989a,b; Carlson, 1989, 1991). In other words, it is unlikely that the garnet of the intermediate size classes grew during multiple crystallization events.

The deviation of population densities of the larger and smallest size classes from the slope in Fig. 7 could indicate that growth of the garnet for these size classes was not governed by the same nucleation and growth mechanisms (or rates) as for crystals of the intermediate size classes (Cashman & Ferry, 1988; Kerrick *et al.*, 1991). This could be inferred from the fact that the nucleation density of garnet grains ($r \leq 0.5$ mm) in the mica-poor layers is much higher than that of garnet grains ($r > 0.5$ mm) in the mica-rich layers. A difference in nucleation density could lead to a difference in growth rate (e.g. Carlson, 1989, 1991). The presence of multiple peaks of X_{Mn} (Fig. 5h) and of multiple inclusion-rich cores (Fig. 4b,c) in some larger grains ($r > 0.5$ mm) suggests that these larger grains may have resulted from impingement of more than two crystals followed by overgrowth (Toriumi, 1986; Ikeda, 1993a). In contrast, a decrease in the number of garnet grains in the smallest size class may be interpreted as a result of suppression of nucleation in diffusion domains during diffusion-influenced nucleation and diffusion-controlled growth (Carlson, 1989, 1991), or a consumption of them due to Ostwald ripening after crystal growth at constant rate (Cashman & Ferry, 1988). However, even if the decrease resulted from Ostwald ripening, the effects of later modification may have been minor, considering a small departure of the population density from the slope in Fig. 7.

Most of the garnet crystals are preferentially distributed within the mica-poor layers, possibly because they were produced by consumption of reactants such as biotite. Most of the garnet grains have diffusion (depletion) haloes (Fig. 4) formed possibly because later nucleation was suppressed in the vicinity of nuclei, which suggests diffusion-controlled growth of the garnet (Fisher, 1978; Ridley & Thompson, 1986; Carlson, 1989, 1991).

In summary, the observations suggest that the garnet grains of intermediate sizes ($c.\ 0.1 \leq r \leq c.\ 0.5$ mm) have been formed by continuous nucleation and diffusion-controlled growth, whereas the smaller ($< c.\ 0.1$ mm) and larger ($> c.\ 0.5$ mm) crystals, the population densities of which deviate from the slope in Fig. 7, have crystallized by different mechanisms or rates. For simplicity, the following analyses are concerned only with crystals of intermediate size ($0.1 \leq r \leq 0.5$ mm).

NUMERICAL ANALYSIS

Through numerical analysis, chemical zoning in garnet grains with different radii developed during the

evolution of M1 metamorphism will be simulated along the T–t path proposed by Okudaira *et al.* (1994), as shown in Fig. 2 and the Appendix. The simulated and observed zoning patterns in garnet grains with different radii from the sillimanite zone will be compared, in order to evaluate the validity of the proposed T–t path for M1.

Analytical model

Growth zoning in regionally metamorphosed garnet is produced by continuous net transfer and exchange reactions driven by changes in P–T conditions (e.g. Loomis & Nimick, 1982; Spear, 1988). If the rate of prograde reactions is assumed to be sufficiently rapid compared with the rate of change in P–T, local equilibrium between the surface of the garnet crystal and matrix is inferred to be maintained throughout metamorphism (Walther & Wood, 1984; Spear, 1988), i.e. components move freely across grain boundaries between garnet and matrix. As mentioned above, textural observations suggest that the garnet grains of intermediate size (*c.* $0.1 \leq r \leq c.$ 0.5 mm) have been formed by diffusion-controlled growth. Therefore, the rate of prograde reactions is inferred to have been much faster than that of intergranular diffusion, because the growth rate of metamorphic minerals is controlled by the slowest rate-limiting process (Fisher, 1978). Consequently, for diffusion-controlled growth, I consider that the rate of intergranular diffusion would be slower than that of prograde metamorphic reactions, although it is rapid enough to justify the boundary conditions on the surface of garnet.

Garnet crystals are grown by net transfer reactions only during the prograde stage, but are never consumed by retrograde net transfer reactions unless an exotic fluid infiltrates the rock. In contrast, cation exchange reactions at the surface of garnet occur during prograde and retrograde stages, and continue until the metamorphic temperature decreases below the closure temperature for cation exchange (Spear, 1989b; Yardley, 1989). Retrograde resorption caused by hydration reactions has been inferred to explain reverse zoning in garnet (e.g. Tracy, 1982). However, because the garnet crystals separated from the metapelite unit are idioblastic and the decrease in the number of the garnet crystals of the smallest size class is small (see Fig. 7), these observations suggest that retrograde resorption of the garnet was minor.

Basic assumptions employed in the analysis are: (1) the garnet statically formed during M1 metamorphism only; (2) nucleation and growth occurred only during the prograde metamorphic stage; (3) the maximum radius of grains crystallized by continuous nucleation and growth is 0.5 mm; (4) growth of the garnets was governed by diffusion-controlled growth; (5) intracrystalline diffusion in the garnet occurred during and after the crystallization; (6) after the thermal peak, the grain size of the garnet did not change; (7) the garnet surface was in equilibrium with adjacent minerals and the composition of the surface was a function of temperature until the metamorphic temperature decreased below the closure temperature for cation exchange; (8) after the temperature fell below the closure temperature, intracrystalline diffusion occurred, being constrained by mass balance within the garnet; and (9) the shapes of garnet crystals are taken as approximately isotropic spheres to simplify the analysis. An explicit finite-difference method with a 1×10^{-5}-m array spacing and a 3.15×10^{7}-s time step was used for the numerical simulation.

Composition of garnet surface

If Tschermak's exchange is ignored, only four independent continuous reactions may operate in the assemblage quartz + plagioclase + K-feldspar + biotite + sillimanite + garnet in the SiO_2–Al_2O_3–FeO–MgO–MnO–CaO–Na_2O–K_2O–H_2O (MnNCKFMASH) system (Spear, 1989a,b), namely

$$FeMg_{-1}\ (\text{garnet}) = FeMg_{-1}\ (\text{biotite}), \tag{1}$$

$$FeMn_{-1}\ (\text{garnet}) = FeMn_{-1}\ (\text{biotite}), \tag{2}$$

$$\underset{\text{(grossular)}}{Ca_3Al_2Si_3O_{12}} + \underset{\text{(sillimanite)}}{2Al_2SiO_5} + \underset{\text{(quartz)}}{SiO_2} = \underset{\text{(anorthite)}}{3CaAl_2Si_2O_8}, \tag{3}$$

$$\underset{\text{(annite)}}{KFe_3AlSi_3O_{12}(OH)_2} + \underset{\text{(sillimanite)}}{Al_2SiO_5} + \underset{\text{(quartz)}}{2SiO_2} = \underset{\text{(almandine)}}{Fe_3Al_2Si_3O_{12}} + \underset{\text{(K-feldspar)}}{KAlSi_3O_8} + H_2O. \tag{4}$$

In general, the manganese component is more concentrated in garnet than in most coexisting minerals, the ratio Mn/(Mn + Fe) decreasing in the order garnet > ilmenite ≫ cordierite > biotite (e.g. Pownceby *et al.*, 1987). Garnet may stably coexist with ilmenite ($FeTiO_3$), which commonly forms a solid solution with pyrophanite ($MnTiO_3$). This suggests the possibility of Fe–Mn partitioning between garnet and ilmenite, according to the following exchange reaction:

$$\underset{\text{(almandine)}}{Fe_3Al_2Si_3O_{12}} + \underset{\text{(pyrophanite)}}{3MnTiO_3} = \underset{\text{(spessartine)}}{Mn_3Al_2Si_3O_{12}} + \underset{\text{(ilmenite)}}{3FeTiO_3}, \tag{5}$$

and this partitioning strongly depends on temperature (Pownceby *et al.*, 1987).

From Spear (1988), a difference in the composition (ΔX_{Mn}) of garnet grown by continuous reactions (Eqs 1–5) may be computed for a difference in temperature

(ΔT) and pressure (ΔP) by the relationship

$$\Delta X_{Mn} = (\partial X_{Mn}/\partial T)_p \Delta T + (\partial X_{Mn}/\partial P)_T \Delta P . \quad (6)$$

Because changes in spessartine component only slightly reflect changes in pressure (Spear, 1989b) and the garnet grains are assumed to have crystallized statically, the second term on the right-hand side of Eq. (6) can be neglected. Therefore, the composition of the surface of the garnet is expected to be a function only of temperature, and the above equation can be rewritten for a certain finite temperature interval as

$$X_{Mn} = (dX_{Mn}/dT)T + C , \quad (7)$$

where T and C are temperature (K) and constant, respectively. (dX_{Mn}/dT) and C are assumed to be -1.0×10^{-3} and 1.095, respectively, to fit the highest and lowest values of X_{Mn} simulated for 0.5-mm garnet after 2 Myr of the system's evolution to those of the observed one. These values correspond with those calculated by the Gibbs method by Spear (1989a) for metamorphic temperatures at which the assemblage garnet + biotite + sillimanite + K-feldspar + quartz + plagioclase is stable, as at Fall Mountain, New Hampshire.

Diffusion-controlled growth

A rate of growth controlled by intergranular diffusion has an exponential dependence upon temperature (Ridley & Thompson, 1986; Carlson, 1989; Kerrick *et al.* 1991). When the ith crystal nucleates at time t_i, its radius r as a function of time t is given by the following general form of the diffusion-controlled growth law (Christian, 1975; Carlson, 1989):

$$r_i(t) = k_1 \sqrt{D_e(t - t_i)} \quad (8)$$

where D_e and k_1 are an effective diffusion coefficient for intergranular diffusion and a dimensionless constant, respectively. According to Carlson (1989), the effective diffusion coefficient D_e at T for intergranular diffusion is written as an Arrhenius type equation:

$$D_e = D_\infty \exp\left(\frac{-E_a}{RT}\right) \quad (9)$$

where D_∞ is the value of the diffusion coefficient at infinite T, which is assumed to be constant, and E_a, R and T are the activation energies for intergranular diffusion, gas constant and temperature (K), respectively. Substituting (9) into (8) gives

$$r_i(t) = k_2 \sqrt{(t - t_i) \exp\left(\frac{-E_a}{RT}\right)} \quad (10)$$

where growth constant k_2 is $k_1\sqrt{(D_\infty)}$, and E_a is taken to be 8.37×10^4 J mol^{-1} (Fisher, 1978). The growth constant k_2 has not previously been estimated by experimental studies. Here, the value of k_2 is assumed by using the following method, which is similar to those adopted by Kretz (1974) and Carlson (1989). In the above mentioned mineral assemblage, garnet can be grown by the reaction biotite + sillimanite + quartz = garnet + K-feldspar + H_2O, at a temperature above the breakdown of muscovite + quartz (Spear, 1989a). Provided that the largest grain radius attainable by diffusion-controlled growth is 0.5 mm during the increase from the breakdown temperature of muscovite + quartz (600 °C) to the highest temperature (670 °C), the growth constant k_2 is obtained as 6.29×10^{-8} m s$^{-0.5}$. The value of the growth constant is fixed for other garnet grains with different radii. Figure 8(b) shows the radius vs. time curves nucleated at different times during the prograde T–t path (Fig. 8a). The average growth rate ranges from 5.1×10^{-6} to 2.9×10^{-5} mm yr^{-1}. The growth rate is comparable with the estimated one (1.3×10^{-6}–1.9×10^{-5} mm yr^{-1}), based on dating of a zoned garnet grain from Pigeon Island, Newfoundland, which probably crystallized by diffusion-controlled growth (Vance & O'Nions, 1990).

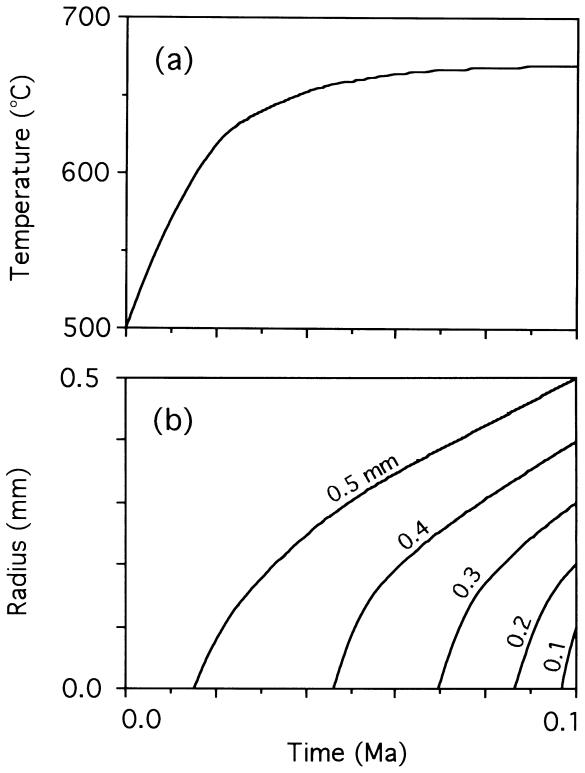

Fig. 8. (a) T–t path during the prograde stage of the path in Fig. 2. (b) Radius–time curves of garnet grains with radii of 0.5 mm (t_i = 0.0150 Myr), 0.4 mm (t_i = 0.0460 Myr), 0.3 mm (t_i = 0.0695 Myr), 0.2 mm (t_i = 0.0865 Myr) and 0.1 mm (t_i = 0.0966 Myr), respectively, corresponding to the T–t path of (a) using Eq. (10). Nucleation of garnet crystals is continuous from the temperature of the breakdown of muscovite + quartz (600 °C) to the highest temperature (670 °C), and growth of the garnet grains is governed by a diffusion–controlled growth law during the above temperature range.

Intracrystalline diffusion

For intracrystalline diffusion in garnet, it is appropriate to apply the model for diffusion in a sphere (Crank, 1975). A fundamental equation to be solved is

$$\frac{\partial X}{\partial t}=\frac{1}{x^2}\frac{\partial}{\partial x}\left(Dx^2\frac{\partial X}{\partial x}\right), \tag{11}$$

with boundary conditions as

$$\frac{\partial X}{\partial x}=0 \text{ at the centre of a sphere},$$

$$X=f(T) \text{ at the outermost margin of a sphere},$$

where X, t, D and x represent concentration of the component, time, diffusion coefficient of the component and distance, respectively.

The garnet is treated as an almandine–spessartine solid solution in the following analyses, because the garnet grains have high (Fe+Mn)/(Fe+Mn+Mg+Ca) ratios, 0.86–0.90 (Table 1), and complementary zoning profiles of spessartine and almandine with relatively small change in pyrope and grossular (Fig. 5). Therefore, the diffusional relaxation of the pattern can be considered to involve essentially Fe–Mn exchange (Elphick *et al.*, 1985; Loomis *et al.*, 1985; Chakraborty & Ganguly, 1992), and the diffusion coefficient of the multicomponent system can be treated as that of a binary (Fe–Mn) system.

According to Loomis *et al.* (1985) and Chakraborty & Ganguly (1992), the diffusion coefficient in all ideal binary ionic solutions can be written as

$$D=\frac{D_1^*D_2^*}{X_1D_1^*+X_2D_2^*}, \tag{12}$$

where D_1^* and D_2^* represent tracer diffusion coefficients of the components 1 and 2, respectively, and X_1 and X_2 ($=1-X_1$) are the concentrations of components 1 and 2, respectively. In this study, the tracer diffusion coefficients of Fe and Mn are expressed as follows (Chakraborty & Ganguly, 1990, 1992):

$$D_{Fe}^*=(6.4\times10^{-4})\exp[-(65.82\times10^3+0.14P)/RT]\ \text{cm}^2\ \text{s}^{-1}, \tag{13a}$$

$$D_{Mn}^*=(5.1\times10^{-4})\exp[-(60.57\times10^3+0.15P)/RT]\ \text{cm}^2\ \text{s}^{-1}, \tag{13b}$$

where P is pressure in bar, and is taken to be 4 kbar.

Figure 9 is a schematic diagram of the changing chemical zoning during and after growth of the garnet. As mentioned above, the garnet is grown by using Eq. (10), as shown in Fig. 8(b), and the composition at the surface of the garnet is calculated by using Eq. (7). Because intracrystalline diffusion operates during and after garnet growth, the molar fraction of spessartine at the centre of the garnet decreases with the system's evolution. The growth of garnet finishes after 0.1 Myr when the metamorphic temperature is highest, and the grain size of the garnet after the thermal peak does not change. The X_{Mn} of the outermost margin of the garnet is calculated by using Eq. (7) until the metamorphic temperature decreases to 600 °C, which is assumed to be the closure temperature for the retrograde exchange reactions. Even after the temperature is decreased below the closure temperature, intracrystalline diffusion in the garnet occurs until 2 Myr, being constrained by mass balance within the garnet. There is no change in X_{Mn} of any crystals after 2 Myr, because the intracrystalline diffusion coefficient is very small below the temperature established at 2 Myr (= 520 °C).

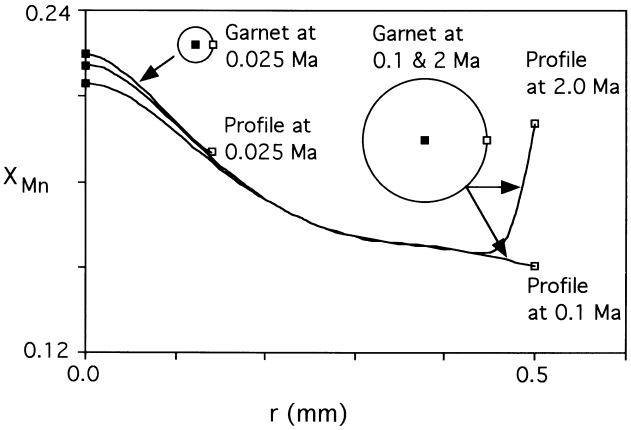

Fig. 9. Schematic diagram showing the changing chemical zoning (X_{Mn}) during and after growth of garnet grain with 0.5 mm radius.

Analytical results

Figure 10 shows simulated zoning profiles of X_{Mn} in garnet grains of different radii (0.1, 0.2, 0.3, 0.4 and 0.5 mm) when growth is complete (thin solid lines) and those after 2 Myr has elapsed after the intrusion (thick solid lines). Important results shown in Fig. 10 are: (1) the smallest grain (0.1 mm in radius) shows reverse zoning from the centre to the outermost margin (Fig. 10a); (2) small grains ($0.2\leq r\leq0.4$ mm) consist of unzoned cores and reversely zoned rims (Fig. 10b–d) and the variations of X_{Mn} in the unzoned parts of the garnet grains with radii of 0.2, 0.3 and 0.4 mm are *c.* 0.13, 0.36 and 0.69 mol%, respectively; (3) the largest grain (0.5 mm in radius) consists of a normally zoned core and reversely zoned rim (Fig. 10e), and the difference between the highest and lowest X_{Mn} is *c.* 5.96 mol%; and (4) the widths of the reversely zoned parts of all the crystals with different radii vary from 0.07 to 0.1 mm.

Comparison between the zoning profiles at the end of growth and those at 2 Myr shows that the unzoned core of smaller garnet grains (Fig. 10b–d) does not really cause diffusional homogenization, but reflects very small reaction progress ($=\Delta X_{Mn}$) in the later formed garnets. That is, the smaller garnet grains have unzoned cores because the very small difference in X_{Mn}

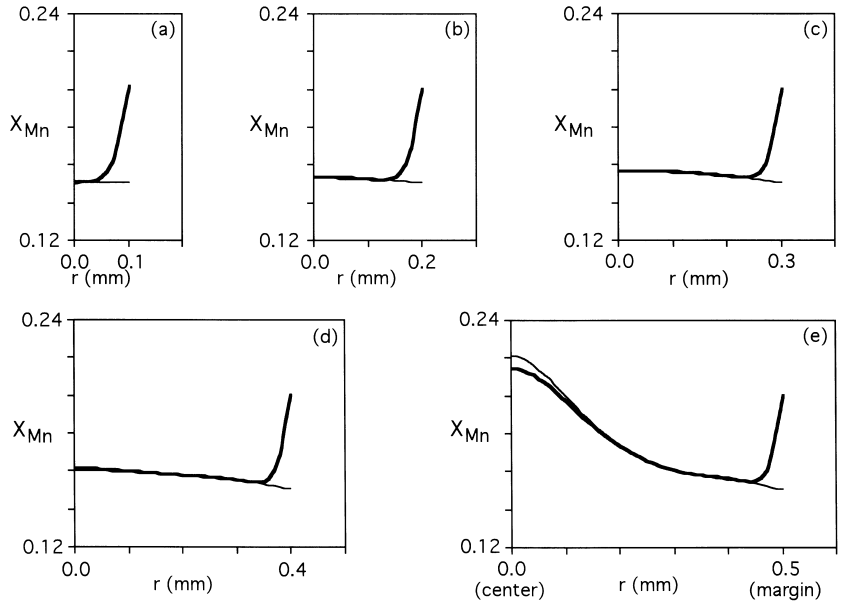

Fig. 10. Simulated chemical zoning patterns of grains with radii: (a) 0.1 mm; (b) 0.2 mm; (c) 0.3 mm; (d) 0.4 mm; and (e) 0.5 mm. Thin and thick solid lines indicate zoning profiles at the end of growth and 2 Myr after the intrusion, respectively.

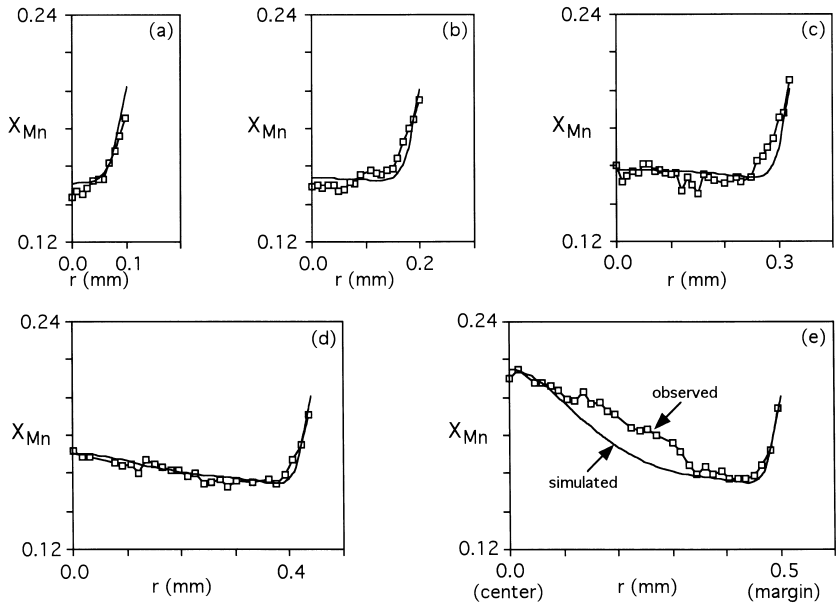

Fig. 11. Observed zoning profiles of garnet grains with different radii, compared with the simulated ones after 2 Myr. (a)–(e) are the same as (a)–(e) in Fig. 5, respectively. Thin solid line with open squares and thin solid line denote observed and simulated zoning profiles, respectively.

resulted from very small change in temperature during their growth. In contrast, the preservation of a distinct normal zoning of X_{Mn} in the garnet grain of 0.5 mm radius (Fig. 10e) results from a relatively large change in temperature during the growth period. The temperature interval (ΔT) during the growth of the 0.5-mm garnet is *c.* 70 °C, although the ΔT during the growth of the garnet grains smaller than 0.40 mm in radius is smaller than *c.* 10 °C (see Fig. 8). These results suggest that the zoning patterns in the cores of all the garnet grains reflect the prograde *T–t* history, although the zoning patterns at the rims of all the garnet grains and near the centre of the largest garnet grain are modified by intracrystalline diffusional relaxation, because of relatively large difference in X_{Mn} within a relatively short distance.

DISCUSSION

Figure 11 shows comparisons between the chemical zoning of the observed garnet grains (0.10, 0.20, 0.32, 0.44 and 0.50 mm in radius) in Fig. 5 and the patterns simulated at 2 Myr in the system's evolution. It indicates that the observed zoning profiles are well reproduced by the numerical model with a difference of less than 1 mol%, except for the largest grain. In the middle part of the largest grain, the values of the simulated X_{Mn} are lower than those of the observed one, with a maximum difference of *c.* 1.7 mol% (Fig. 11e). The difference between the observed and simulated zoning patterns in the garnet may have resulted from differences between the actual and proposed *T–t* paths. According to Okudaira *et al.*

(1993), the highest temperature for rocks in the sillimanite zone could have ranged between 630 and 690 °C. It is therefore necessary to examine possible variations in the zoning patterns for a range of T–t paths. To examine the variation of garnet zoning, temperatures of different T–t paths are taken to be proportional to those of the previously simulated one (Fig. 2). Hence, temperatures of the different path to be examined here are given by

$$T_1 = T_0 + (T_0 - 773)f \qquad (14)$$

where T_0 and T_1 represent the temperature (K) of the previously estimated path (Fig. 2) and that of the modified one, respectively, and f is a scaling factor. Figure 12(a) shows the modified T–t path (thin solid line) between 0 and 2 Myr with f of -0.12, which corresponds to a 20 °C decrease in the thermal peak from the previously estimated one (thick solid line). Figure 12(b) represents the modified zoning profile of X_{Mn} in the simulated garnet grain of 0.5 mm radius

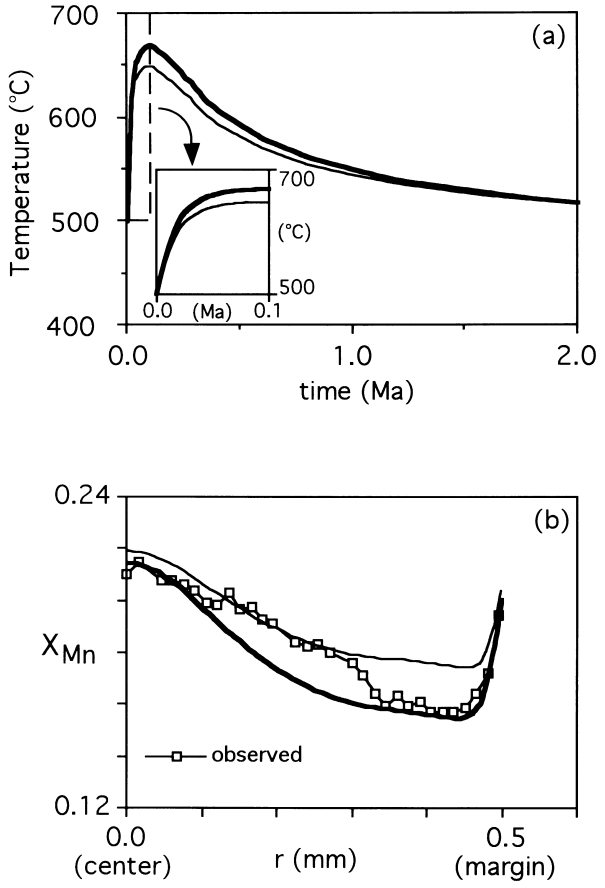

Fig. 12. (a) T–t plots between 0 and 2 Myr, to examine possible variations in zoning patterns for different T–t paths. Thick solid line represents the same path ($f=0$) as in Fig. 2. Thin solid line shows the path with $f=-0.12$. (b) Plots of X_{Mn} versus distance (in mm) for the garnet with 0.5 mm radius simulated for the previously estimated path (thick solid line) and the modified one (thin solid line). Thin solid line with open squares denote the observed zoning profile for the garnet grain with 0.5 mm radius (sample E).

(thin solid line) calculated for the modified path. In this calculation, the same assumptions are employed as those of the previous ones, except for the values of k_2 and t_i. As shown in Fig. 12(b), the observed zoning pattern for the 0.5-mm-radius garnet grain (thin solid line with open squares) falls between the profiles calculated for the modified T–t path and for the previously estimated one. This result indicates that the difference in the peak temperature between the numerically simulated T–t path and the actual T–t path was probably less than 20 °C. Furthermore, the maximum difference between the observed and simulated X_{Mn} occurs in the middle part of the garnet grain, which may suggest that the temperatures of the actual T–t path are lower than those of the proposed one at the early to middle stages (*c.* 0.02–0.06 Myr) of the prograde metamorphism.

As mentioned above, the observed X_{Mn} at the centre of garnet grains ranging from *c.* 0.1 to 0.4 mm in radius (solid squares in Fig. 13) increases slightly with grain size, although the X_{Mn} value of garnet grains with similar grain size varies by *c.* 1 mol%. In contrast, for the grains with a radius greater than *c.* 0.4 mm, the increase of the X_{Mn} values with grain size is abrupt. Such a sharp increase has been reported by Kretz (1973) for a garnet–biotite–cordierite schist near Yellowknife, Canada. The X_{Mn} at the centre of the simulated garnet grains (solid line in Fig. 13) also slightly changes for the sizes between *c.* 0.1 and 0.4 mm, and abruptly increases for the sizes greater than *c.* 0.4 mm. Overall, the values of X_{Mn} at the centre of the simulated garnet grains are comparable with those of the observed ones, and the difference is less than about 1 mol%, which corresponds to a difference in temperature of *c.* 10 °C calculated by using Eq. (7). In the

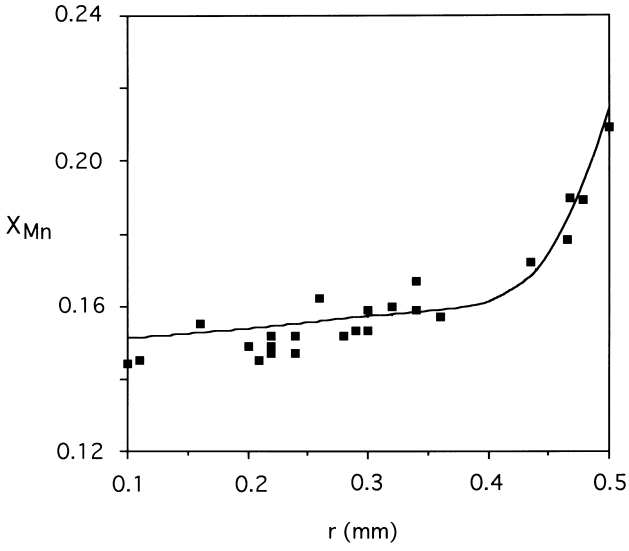

Fig. 13. Observed and simulated X_{Mn} values at the geometrical centres of the garnet grains between 0.1 and 0.5 mm in radius. Solid squares: observed X_{Mn} values. Line: simulated X_{Mn} values at 2 Myr after the intrusion.

garnet grains smaller than *c*. 0.25 mm radius, the values of X_{Mn} at the centre of the simulated garnet grains are systematically higher than those of the observed ones by about 1 mol%. Possible reasons for the difference between the observed and simulated centre X_{Mn} are that (1) the value of dX_{Mn}/dT in Eq. (7) is underestimated or (2) the temperatures of the proposed T–t path are lower than those of the actual path in the later stages of prograde metamorphism. If (2) is correct, the actual metamorphic temperatures may be higher than the proposed ones by *c*. 10 °C at a late stage (*c*. 0.08–0.1 Myr) of the prograde metamorphism.

SUMMARY AND CONCLUSIONS

Garnet crystals from the LPHT Ryoke metamorphic belt in the Yanai district, south-western Japan, show various chemical zoning patterns. The zoning pattern at the core of the garnet grains systematically varies from reversely zoned, through unzoned, to normally zoned patterns with increasing grain size of the garnet. Quantitative and qualitative textural analyses of the garnet grains lead to the conclusion that the crystallization mechanism for garnet grains of $0.1 \leq r \leq 0.5$ mm radius is continuous nucleation and diffusion-controlled growth. Chemical zoning of garnet grains with different radii is simulated for the previously estimated T–t path (Okudaira *et al.* 1994) using a numerical model of continuous nucleation and diffusion-controlled growth, in combination with intracrystalline diffusion. The results of the simulation indicate that the observed zoning patterns of the various sizes of garnet are well reproduced by the numerical model, in spite of the fact that simulated zoning patterns strongly depend on T–t history, i.e. X_{Mn} changes responding to subtle changes in temperature. From a comparison of observed and simulated X_{Mn} for the T–t path, the temperatures of the actual T–t path could have been lower than those of the proposed one by *c*. 20 °C at the early to middle stages, and are higher by *c*. 10 °C at the late stage of the prograde metamorphism. Thus, if the employed analytical model and the assumed value of the parameters are appropriate, the results of this study suggest that the proposed T–t path is valid for the low-P Ryoke metamorphism.

ACKNOWLEDGEMENTS

I thank I. Hara, K. Hoshino and Y. Iwase for assistance in the work. I also thank A. Minami for assistance with the electron-probe analyses at the Instrument Centre for Chemical Analysis, Hiroshima University. S. Banno, T. Nishiyama, J. C. Schumacher, T. Takeshita and M. Toriumi are thanked for critical reading and useful comments of an early version of the manuscript. The paper benefited substantially from detailed reviews by B. J. Hensen and F. S. Spear. R. H. Vernon is thanked for the editorial handling of the manuscript.

REFERENCES

Banno, S. & Nakajima, T., 1992. Metamorphic belts of Japanese Islands. *Annual Reviews of Earth and Planetary Sciences*, **20,** 159–179.

Banno, S., Sakai, C. & Higashino, T., 1986. Pressure–temperature trajectory of the Sanbagawa metamorphism deduced from garnet zoning. *Lithos*, **19,** 51–63.

Barker, A. J., 1990. *Introduction to Metamorphic Textures and Microstructures*. Blackie, New York.

Bergantz, G. W., 1991. Physical and chemical characterization of plutons. In: *Contact Metamorphism* (ed. Kerrick D. M.), *Reviews in Mineralogy*, **26,** 13–42.

Carlson, W. D., 1989. The significance of intergranular diffusion to the mechanisms and kinetics of porphyroblast crystallization. *Contributions to Mineralogy and Petrology*, **103,** 1–24.

Carlson, W. D., 1991. Competitive diffusion-controlled growth of porphyloblasts. *Mineralogical Magazine*, **55,** 317–330.

Cashman, K. V. & Ferry, J. M., 1988. Crystal size distribution (CSD) in rocks and the kinetics and dynamics of crystallization III. Metamorphic crystallization. *Contributions to Mineralogy and Petrology*, **99,** 401–415.

Chakraborty, S. & Ganguly, J., 1990. Compositional zoning and cation diffusion in garnets. In: *Diffusion, Atomic Ordering,* and *Mass Transport, Selected Topics in Geochemistry* (ed. Ganguly, J.), *Advances in Physical Geochemistry*, **8**, 120–175.

Chakraborty, S. & Ganguly, J., 1992. Cation diffusion in aluminosilicate garnets: experimental determination in spessartine–almandine diffusion couples, evaluation of effective binary diffusion coefficients, and applications. *Contributions to Mineralogy and Petrology*, **111,** 74–86.

Christian, J. W., 1975. *The Theory of Transformations in Metals and Alloys: Part 1 – Equilibrium and General Kinetic Theory* (2nd edn). Pergamon Press, Oxford.

Crank, J., 1975. *The Mathematics of Diffusion* (2nd edn). Oxford University Press, London.

Dempster, T. J., 1985. Garnet zoning and metamorphism of the Barrovian Type Area, Scotland. *Contributions to Mineralogy and Petrology*, **89,** 30–38.

De Yoreo, J. J., Lux, D. R. & Guidotti, C. V., 1989. The role of crustal anatexis and magma migration in the thermal evolution of regions of thickened continental crust. In: *Evolution of Metamorphic Belts* (eds Daly, J. S., Cliff, R. A. & Yardley, B.W.D.). *Geological Society Special Publications*, **43**, 187–202.

Elphick, S. C., Ganguly, J. & Loomis, T. P., 1985. Experimental determination of cation diffusivities in aluminosilicate garnets I. Experimental methods and interdiffusion data. *Contributions to Mineralogy and Petrology*, **90,** 36–44.

England, P. C. & Thompson, A. B., 1984. Pressure–temperature–time paths of regional metamorphism I. Heat transfer during the evolution of regions of thickened continental crust. *Journal of Petrology*, **25,** 894–928.

Fisher, G. W., 1978. Rate laws in metamorphism. *Geochimica et Cosmochimica Acta*, **42,** 1035–1050.

Florence, F. P. & Spear, F. S., 1991. Effects of diffusional modification of garnet growth zoning on P–T calculations. *Contributions to Mineralogy and Petrology*, **107,** 487–500.

Florence, F. P. & Spear, F. S., 1993. Influences of reaction history and chemical diffusion on P–T calculations for staurolite schists from the Littleton Formation, northwestern New Hampshire. *American Mineralogist*, **78,** 345–359.

Green, T. H., 1992. Experimental phase equilibrium studies of garnet-bearing I-type volcanics and high-level intrusives from Northland, New Zealand. *Transactions of Royal Society of Edinburgh: Earth Sciences*, **83,** 429–438.

Hanson, R. B., 1992. Effects of fluid production on fluid flow during regional and contact metamorphism. *Journal of Metamorphic Geology*, **10,** 87–97.

Hanson, R. B. & Barton, M. D., 1989. Thermal development of low-pressure metamorphic belts: Results from two-dimensional numerical models. *Journal of Geophysical Research*, **94,** 10363–10377.

Hara, I., Sakurai, Y., Okudaira, T., Hayasaka, Y., Ohtomo, Y. & Sakakibara, N., 1991. Tectonics of the Ryoke belt. *Excursion Guidebook of 98th Annual Meeting of Geological Society of Japan*, pp. 1–20 (in Japanese). Geological Society of Japan.

Higashimoto, S., Nureki, T., Hara, I., Tsukuda, E. & Nakajima, T., 1983. *Geology of the Iwakuni district. Quadrangle series, scale, 1:50,000*. Geological Survey of Japan (in Japanese with English abstract).

Hodges, K. V. & Silverberg, D. S., 1988. Thermal evolution of the Greater Himalayas, Garhwal, India. *Tectonics*, **7,** 583–600.

Honma, H., 1974. Major element chemistry of metamorphic and granitic rocks of the Yanai district in the Ryoke belt. *Journal of Mineralogy, Petrology, and Economic Geology*, **69,** 193–204.

Ikeda, T., 1991. Heterogeneous biotite from Ryoke metamorphic rocks in the Yanai district, southwest Japan. *Journal of Geological Society of Japan*, **97,** 537–547.

Ikeda, T., 1993a. Compositional zoning patterns of garnet during prograde metamorphism from the Yanai district, Ryoke metamorphic belt, southwest Japan. *Lithos*, **30,** 109–122.

Ikeda, T., 1993b. Homogenization of chemical zoning of garnet of the Ryoke metamorphic rocks from the Yanai district. *Earth Monthly*, **15,** 164–167 (in Japanese).

Jaeger, J. C., 1964. Thermal effects of intrusions. *Reviews of Geophysics*, **2,** 44–54.

Kagami, H., Iizumi, S., Tainosho, Y. & Owada, M., 1992. Spatial variations of Sr and Nd isotope ratios of Cretaceous–Paleogene granitoid rocks, southwest Japan arc. *Contributions to Mineralogy and Petrology*, **112,** 165–177.

Kerrick, D. M., Lasaga, A. C. & Raeburn, S. P., 1991. Kinetics of heterogeneous reactions. In: *Contact Metamorphism* (ed. Kerrick, D. M.), *Reviews in Mineralogy*, **26**, 583–672.

Kretz, R., 1973. Kinetics of the crystallization of garnet at two localities near Yellowknife. *Canadian Mineralogist*, **12,** 1–20.

Kretz, R., 1974. Some models for the rate of crystallization of garnet in metamorphic rocks. *Lithos*, **7,** 123–131.

Loomis, T. P., 1983. Compositional zoning of crystal: a record of growth and reaction history. In: *Kinetics* and *Equilibrium in Mineral Reaction* (ed. Saxena, S. K.), *Advances in Physical Geochemistry*, **3**, 1–61.

Loomis, T. P., Ganguly, J. & Elphick, S. C., 1985. Experimental determination of cation diffusivities in aluminosilicate garnets II. Multicomponent simulation and tracer diffusion coefficients. *Contributions to Mineralogy and Petrology*, **90,** 45–51.

Loomis, T. P. & Nimick, F. B., 1982. Equilibrium in Mn–Fe–Mg aluminous pelitic compositions and the equilibrium growth of garnet. *Canadian Mineralogist*, **20,** 393–410.

Loosveld, R. J. H., 1989. The synchronism of crustal thickening and low-pressure facies metamorphism in the Mount Isa Inlier, Australia 2. Fast convective thinning of mantle lithosphere during crustal thickening. *Tectonophysics*, **165,** 191–218.

Lux, D. R., De Yoreo, J. J., Guidotti, C. V. & Decker, E. R., 1986. The role of plutonism in low-pressure/high-temperature metamorphic belt formation. *Nature*, **323,** 794–797.

Miyashiro, A., 1961. Evolution of metamorphic belts. *Journal of Petrology*, **2,** 277–311.

Morishita, R., 1992. Crystal size distribution of Togawa andesite lava. *Bulletin of Volcanological Society of Japan*, **37,** 285–293 (in Japanese with English abstract).

Nakajima, T., 1994. The Ryoke plutonometamorphic belt: crustal section of the Cretaceous Eurasian continental margin. *Lithos*, **33,** 51–66.

Nakajima, T., Williams, I. S. & Watanabe, T., 1993. SHRIMP U–Pb ages of the Ryoke and San-yo granitoids in Southwest Japan, *Abstracts with Programs, 100th Annual Meeting of Geological Society of Japan*, 584 (in Japanese).

Nureki, T., 1960. Structural investigation of the Ryoke metamorphic rocks of the area between Iwakuni and Yanai, Southwestern Japan. *Journal of Science of Hiroshima University, Series C*, **3,** 69–141.

Okamura, Y., 1960. Structural and petrological studies on the Ryoke gneiss and granodiorite of the Yanai district, Southwest Japan. *Journal of Science of Hiroshima University, Series C*, **3,** 143–213.

Okudaira, T., Hara, I., Sakurai, Y. & Hayasaka, Y., 1993. Tectono-metamorphic processes of the Ryoke belt in the Iwakuni-Yanai district, southwest Japan. In: *Evolution of the Arc Crust in Southwest Japan* (eds Komatsu, M., Takeshita, T. & Sakakibara, M.), *Memoirs of Geological Society of Japan*, **42**, 91–120.

Okudaira, T., Hara, I. & Takeshita, T., 1994. Thermal modeling for the low-pressure facies series Ryoke metamorphism. *Earth Monthly*, **16,** 486–489 (in Japanese).

Okudaira, T., Takeshita, T., Hara, I. & Ando, J., 1995. A new estimate of the conditions for transition from basal $< a >$ to prism [c] slip in naturally deformed quartz. *Tectonophysics*, **250,** 31–46.

Oxburgh, E. R. & Turcotte, D. L., 1971. Origin of paired metamorphic belts and crustal dilation in island arc regions. *Journal of Geophysical Research*, **76,** 1315–1327.

Peacock, S. M., 1989. Numerical constraints on rates of metamorphism, fluid production, and fluid flux during regional metamorphism. *Geological Society of America Bulletin*, **101,** 476–485.

Powneby, M. I., Wall, V. J. & O'Neill, H.St.C., 1987. Fe–Mn partitioning between garnet and ilmenite: experimental calibration and applications. *Contributions to Mineralogy and Petrology*, **97,** 116–126.

Ridley, J. & Thompson, A. B., 1986. The role of mineral kinetics in the development of metamorphic microtextures. In: *Fluid–Rock Interactions During Metamorphism* (eds Walther, J. V. & Wood, B. J.), *Advances in Physical Geochemistry*, **5**, 154–193.

Rothstein, D. A. & Hoisch, T. D., 1994. Multiple intrusions and low-pressure metamorphism in the central Old Woman Mountains, south-eastern California: constraints from thermal modelling. *Journal of Metamorphic Geology*, **12,** 723–734.

Shigeno, H. & Yamaguchi, M., 1976. A Rb-Sr isotopic study of metamorphism and plutonism in the Ryoke belt, Yanai district, Japan. *Journal of Geological Society of Japan*, **82,** 687–698 (in Japanese with English abstract).

Spear, F. S., 1988. Metamorphic fractional crystallization and internal metasomatism by diffusional homogenization of zoned garnets. *Contributions to Mineralogy and Petrology*, **99,** 507–517.

Spear, F. S., 1989a. Relative thermobarometry and metamorphic P–T paths. In: *Evolution of Metamorphic Belts* (eds Daly, J. S., Cliff, R. A. & Yardley, B.W.D.), *Geological Society Special Publication*, **43**, 63–82.

Spear, F. S., 1989b. Petrologic determination of metamorphic pressure–temperature–time paths. In: *Metamorphic Pressure–Temperature–Time Paths* (eds Spear, F. S. & Peacock, S.M.), *Short Course in Geology*, **7**, 1–55.

Spear, F. S., 1991. On the interpretation of peak metamorphic temperatures in light of garnet diffusion during cooling. *Journal of Metamorphic Geology*, **9,** 379–388.

Spear, F. S., 1993. *Metamorphic Phase Equilibria and Pressure–Temperature–Time Paths*. Mineralogical Society of America, Washington, DC.

Spry, A., 1969. *Metamorphic Textures*. Pergamon Press, Oxford.

Sugimura, A. & Uyeda, S., 1973. *Island arcs, Japan and its environs. Development of Geotectonics, 3*. Elsevier, Amsterdam.

Suzuki, K., Adachi, M & Kajizuka, I., 1994. Electron microprobe observations of Pb diffusion in metamorphosed detrital monazites. *Earth and Planetary Science Letters*, **128,** 391–405.

Thompson, J.B., 1957. The graphical analysis of mineral assemblages in pelitic schists. *American Mineralogist*, **42,** 842–858.

Toriumi, M., 1986. Mechanical segregation of garnet in synmetamorphic flow of pelitic schists. *Journal of Petrology*, **27,** 1395–1408.

Tracy, R. J., 1982. Compositional zoning and inclusions in metamorphic minerals. In: *Characterization of Metamorphism through Mineral Equilibria* (ed. Ferry, J. M.), *Reviews in Mineralogy*, **10**, 355–397.

Turcotte, D. L. & Schubert, G., 1982. *Geodynamics*. John Wiley & Sons, New York.

Vance, D. & O'Nions, R. K., 1990. Isotopic chronometry of zoned garnets: growth kinetics and metamorphic histories. *Earth and Planetary Science Letters*, **97,** 227–240.
Walther, J. V. & Orville, P. M., 1982. Volatile production and transport in regional metamorphism. *Contributions to Mineralogy and Petrology*, **79,** 252–257.
Walther, J. V. & Wood, B. J., 1984. Rate and mechanism in prograde metamorphism. *Contributions to Mineralogy and Petrology*, **88,** 246–259.
Wells, P. R. A., 1980. Thermal models for the magmatic accretion and subsequent metamorphism of continental crust. *Earth and Planetary Science Letters*, **46** 253–265.
Wickham, S. M. & Oxburgh, E. R., 1987. Low-pressure regional metamorphism in the Pyrenees and its implications for the thermal evolution of rifted continental crust. *Philosophical Transactions of Royal Society of London*, **A321**, 219–242.
Yardley, B. W. D., 1977. An empirical study of diffusion in garnet. *American Mineralogist*, **62,** 793–800.
Yardley, B. W. D., 1989. *An Introduction to Metamorphic Petrology*. Longman Scientific & Technical, Essex, England.

Received 22 December 1994; revision accepted 19 December 1995.

APPENDIX

Thermal modelling for M1 metamorphism

The thermal model for M1 metamorphism proposed by Okudaira *et al.* (1994) is as follows. A one-dimensional heat transfer equation with fluid advection term is written as

$$\rho_m C_m \frac{\partial T}{\partial t} = K\frac{\partial^2 T}{\partial z^2} - C_f \frac{\partial (Tu)}{\partial z} + A \qquad \text{(A1)}$$

where ρ_m = density of rock (2750 kg m^{-3}); C_m = specific heat of rock (880 J kg^{-1} K^{-1}); T = temperature (K); t = time (s); K = thermal conductivity (2.8 W m^{-1} K^{-1}); z = vertical coordinate measured from the earth's surface (m); C_f = specific heat of fluid (3750 J kg^{-1} K^{-1}); u = mass fluid flux (kg m^{-2} s^{-1}); and A is heat production of radioactive elements (W m^{-3}). Equation (A1) is solved numerically using an explicit finite-difference method with a 1000-m array spacing (Δz) and a 3.15×10^9-s time step (Δt).

The boundary conditions are a constant temperature at the earth's surface and constant mantle heat flux q_m at the bottom of the lithosphere. The thickness of the lithosphere before the intrusion of the Older Ryoke granitoid sheet is assumed to be 30 km. The initial geotherm in the lithosphere is assumed to be *c.* 30 °C km^{-1}, based on the P–T conditions of M0 metamorphism, corresponding to q_m of 0.08 W m^{-2}. The initial geothermal gradient (*c.* 30 °C km^{-1}) is comparable with the mean geothermal gradient of an active continental margin or an island arc (Sugimura & Uyeda, 1973).

The Older Ryoke granitoid sheet was emplaced at the middle layer between the sillimanite and garnet zones (Okudaira *et al.,* 1993). Based on the inferred pressures of the sillimanite and garnet zones, the granitoid sheet is assumed to have been emplaced between 16 and 19 km. In the numerical simulation, it is assumed that the sheet is 3 km thick, of granodioritic composition, and emplaced instantaneously. After the intrusion, the thickness of the lithosphere instantaneously increases to 35 km. According to Hanson & Barton (1989), I have used the crystallization interval between 950 and 750 °C to estimate the initial intrusion temperature of 900 °C for the granodioritic composition. The initial fluid content of the magma is taken to be 4 wt%, following Bergantz (1991) and Green (1992). The crystallizing magma produces heat (latent heat) during the crystallization interval. Production of heat by the crystallizing magma is taken to be 3.35×10^5 J kg^{-1} according to Wells (1980).

In the wall rocks, most dehydration reactions are endothermic and thus consume heat (Peacock, 1989; Spear, 1993). For typical dehydration reactions, the ΔH of reaction is in the range of 60–100 kJ per mole of volatile evolved (Walther & Orville, 1982). During metamorphism, a typical metapelite loses $\approx$5 wt% H_2O (Walther & Orville, 1982), which is equivalent to $\approx 7.6 \times 10^3$ mol m^{-3} of rock. Assuming 60 kJ mol^{-1} for dehydration reactions results in a heat sink of 1.6×10^5 J kg^{-1} (Peacock, 1989). The dehydration reaction interval between 350 and 800 °C is used. It is assumed that rocks initially at temperatures below 350 °C contain 5 wt% volatiles, and rocks initially at temperatures above 800 °C contain no volatiles. For rocks initially at the temperatures within the reaction interval, the volatile content is calculated from eq. (3) in Peacock (1989).

The production of heat by the magmatic crystallization and consumption of heat by the endothermic reactions are calculated assuming that they are a continuous linear function of temperature between the crystallization interval and between the endothermic reaction interval, respectively. The production and consumption of heat are incorporated into the numerical model using an effective heat capacity and an effective thermal diffusivity for the rocks (Jaeger, 1964; Hanson & Barton, 1989; Peacock, 1989). The second term on the right-hand side of Eq. (A1) indicates heat transport by advection. The fluid flux produced by the crystallization of the magma and by the dehydration reactions is calculated using the methods of Peacock (1989) and Hanson (1992). Radiogenic heat production, the third term on the right-hand side of Eq. (A1), is calculated by using eq. (4–24) in Turcotte & Schubert (1982).

The results of the simulated peak temperatures for the cordierite, sillimanite and garnet zones are well within the limits of the petrologically estimated ones (Okudaira *et al.*, 1993, 1995). The simulated and petrologically estimated metamorphic field gradients are also consistent. Therefore, the T–t path is used as a standard T–t path for M1 metamorphism in this study. The simulated T–t path for the sillimanite zone is shown in Fig. 2.